Weather and Climate Extremes 41 (2023) 100573

Contents lists available at ScienceDirect

Weather and Climate Extremes

journal homepage: www.elsevier.com/locate/wace

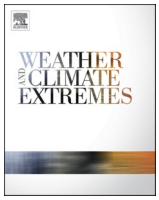

# Identical hierarchy of physical drought types for climate change signals and uncertainty

Parisa Hosseinzadehtalaei [a,*], Bert Van Schaeybroeck [b], Piet Termonia [a,b], Hossein Tabari [b,c]

[a] Department of Physics and Astronomy, Ghent University, Ghent, Belgium
[b] Department of Meteorological and Climate Research, Royal Meteorological Institute of Belgium, Uccle, Belgium
[c] Faculty of Applied Engineering, University of Antwerp, Antwerp, Belgium

ARTICLE INFO

*Keywords:*
Meteorological drought
Hydrological drought
Agricultural drought
Climate change impact assessment
Uncertainty analysis

ABSTRACT

Climate change may have different impacts on different types of drought through its influence on the mechanisms of the propagation of a precipitation lack into a hydrological or agricultural drought. The involvement of additional processes in runoff and soil moisture modeling potentially leads to discrepancies in the projection uncertainties and signal-to-noise ratios between different drought types. This global study compares climate change signals, uncertainty, and signal-to-noise ratios between meteorological, hydrological, and agricultural droughts characterized by standardized precipitation index (SPI), standardized runoff index (SRI), and standardized soil moisture index (SSI), respectively. The comparison is made for five drought characteristics including median and peak intensity, median and longest duration, and frequency using 18 Coupled Model Intercomparison Project Phase 6 (CMIP6) models for four Shared Socioeconomic Pathways (SSPs) SSP1-2.6, SSP2-4.5, SSP3-7.0, and SSP5-8.5. We find that the spatial extent and magnitude in all five drought characteristics increase from meteorological to hydrological to agricultural drought. This increase manifests itself, however, at the expense of augmented uncertainty, to the extent that uncertainty for agricultural drought is up to sevenfold larger compared to meteorological drought. Despite the augmentation of uncertainty from meteorological to agricultural drought, the hierarchy of drought types for climate change signals still holds for the spatial extent of significant signal-to-noise ratios.

## 1. Introduction

Recent years have witnessed a number of severe drought events e.g., the 2011–2012 Eastern Africa drought, the 2011–2017 California drought, the 2018–2022 Southern African drought, the 2019–2020 Australian drought, and the 2022 European drought. The occurrence of such severe drought events has been increasing at an alarming rate, causing profound social, economic, and environmental impacts worldwide (IPCC, 2022). More frequent, longer, and severe droughts during recent decades in large parts of the Americas, Africa, and Asia have been attributed to anthropogenic factors (Chiang et al., 2021). For instance, anthropogenic climate change was found to at least quintupled the risk of the 2015 drought in India (Zachariah et al., 2022). This pattern is expected to persist and the events become worse in the coming decades and towards the end of the 21st century (Tabari and Willems, 2018; Ahmadalipour et al., 2019; van der Wiel et al., 2021; Tabari et al., 2021; Pokhrel et al., 2021). There is high confidence that, across the 21st century, the total exposed area to drought will expand and droughts will become more severe and frequent (IPCC, 2022).

Three physical drought types are commonly recognized in the scientific literature: meteorological, agricultural, and hydrological (Chen et al., 2022). A drought event normally starts with a shortage of precipitation (known as meteorological drought) that may propagate, as it lingers, into a deficit of soil moisture (agricultural drought) and streamflow, reservoir levels, and groundwater (hydrological drought). Meteorological droughts are, however, not always propagated to soil moisture droughts, as such transition depends on many processes affecting the surface water balance (Berg and Sheffield, 2018). When the anomaly of precipitation propagates through the hydrological system, it can be intensified or diminished by other processes at the surface or the land-atmosphere interface (Cook et al., 2018), leading to hydrological and agricultural droughts of different severities. For instance, higher air temperatures can increase evaporative demand which, in turn, increases evaporative losses from the surface, resulting in higher soil-moisture

* Corresponding author.
*E-mail address:* parisa.hosseinzadehtalaei@ugent.be (P. Hosseinzadehtalaei).

https://doi.org/10.1016/j.wace.2023.100573
Received 9 January 2023; Received in revised form 17 May 2023; Accepted 24 May 2023
Available online 25 May 2023

deficits (Berg et al., 2017). Some land-surface and plant processes can also modulate the manifestation of precipitation droughts in the soil, including the reduced plant stomatal conductance in case of drought stress or the increased vegetation total water use efficiency under elevated atmospheric CO2 (Milly and Dunne, 2016; Mankin et al., 2019). These processes induce feedbacks on the near-surface climate that may vary geographically due to variations in vegetation (e.g., phenology, land cover) and land surface properties (e.g., soil moisture content, soil type, topography) (Lauenroth et al., 2014), leading to spatially-dependent susceptibilities across the three drought types.

The complexity of drought propagation processes and the diversity of the propagation over different regions raise the question of how different drought types respond to climate change. Understanding which drought type is more sensitive to climate change may allow the identification of socio-economic sectors impacted by future changes in drought intensity, duration, and frequency. Moreover, distinguishing the areas where the discrepancies among the drought types are more pronounced may advance our understanding (or identify knowledge gaps) of the complex land and atmosphere processes behind the changes. Climate model projections of precipitation are uncertain and vary geographically (Lehner et al., 2020) and latitudinally (Tabari et al., 2019). For soil and runoff, climate models need to simulate soil, landscape, and vegetation attributes apart from climate processes which can add an extra tier of uncertainty to their projections (Schlaepfer et al., 2017).

The accuracy of models in representing the essential processes related to various drought types is critical in assessing their reliability in projecting future changes in drought characteristics. In the Coupled Model Intercomparison Project Phase 6 (CMIP6), these processes are either explicitly represented or parameterized using mathematical equations and empirical relationships. Some models explicitly simulate the atmosphere's response to changes in soil moisture and vegetation cover, while others use parameterizations to represent these processes. Land surface models (LSMs) in CMIP6 simulate soil moisture, soil temperature, and evapotranspiration using physically-based equations that describe water and energy fluxes at the land-atmosphere interface. LSMs also represent vegetation dynamics and carbon cycle processes, affecting the exchange of water and energy between the land and atmosphere (Strebel et al., 2022). However, there are still significant differences between models in their representations of key processes, resulting in varying simulations of runoff and soil moisture even when driven with the same external forcings (Arora et al., 2023). These differences can be due to variations in model structure, parameterization choices, and input data, as well as uncertainties in the underlying physical processes themselves (Fisher and Koven, 2020). Moreover, differences between Earth System Models (ESMs) and General Circulation Models (GCMs) can also be significant, with ESMs including more detailed representations of land surface processes, biogeochemical cycling, and other Earth system components, while GCMs typically focus more on atmospheric dynamics and radiative transfer (Séférian et al., 2019; Lu et al., 2019).

The CMIP6 models represent a significant improvement over the CMIP5 models, with several enhancements in various areas. These include higher-resolution grids, more advanced parameterizations of physical processes, and increased use of observational data for model initialization and evaluation (Eyring et al., 2016, 2019). Specifically, the CMIP6 models offer improved representations of clouds, aerosols, and their interactions, which affect precipitation and evaporation, as well as more sophisticated representations of land surface processes such as vegetation dynamics and biogeochemical cycling, affecting soil moisture and runoff (van den Hurk et al., 2016). Additionally, many of the models now include realistic processes describing the lake–atmosphere interactions, as climate impacts of lakes become more prominent with increasing model horizontal resolution (Lu et al., 2019). Overall, the CMIP6 ensemble produces reasonable simulations for the climatology, spatial distribution, and annual cycle characteristics of soil moisture (Qiao et al., 2022) and for the spatial distribution of the number of dry days and meteorological drought frequency (Coppola et al., 2021). In comparison to the CMIP5 ensemble, the CMIP6 ensemble shows improvements in soil moisture simulations (Yuan et al., 2021) and meteorological drought frequency, particularly over Africa (Coppola et al., 2021). However, despite these improvements, uncertainties and biases still exist, and better representations of drought processes and land surface feedbacks do not necessarily translate into reduced uncertainties in drought risk projections (Cook et al., 2020). Therefore, it is crucial to understand how projection uncertainties differ across various types of drought.

Much of the existing research on the impacts of climate change on global droughts has focused on a separate analysis of meteorological (Spinoni et al., 2020; Ukkola et al., 2020; Wang et al., 2021; Tabari et al., 2021; Li et al., 2021), hydrological (Prudhomme et al., 2014; Wanders and Wada, 2015; Wang et al., 2021), and agricultural (Berg and Sheffield, 2018; Lu et al., 2019; Joo et al., 2020; Tabari and Willems, 2022; Ji et al., 2022) droughts. These studies have used different types of datasets, drought indicators, climate models, and scenarios which hinders drawing a perspective on the discrepancies of the results across different drought types. Several global studies have compared climate change impacts among different drought types but based their analysis on the older generations of global climate models, i.e., the simulations of the CMIP3 GCMs or Hadley Centre models (HadAM3 and HadCM3C) under the Special Report on Emissions Scenarios (SRES) (Burke and Brown, 2008; Taylor et al., 2013), the CMIP5 GCMs under Representative Concentration Pathways (RCPs) (Orlowsky and Seneviratne, 2013; Touma et al., 2015; Wartenburger et al., 2017; Ukkola et al., 2018; Vicente-Serrano et al., 2020), and the simulations from the Inter-Sectoral Impact Model Inter-Comparison Project (ISIMIP) models forced by a limited number (4–5) of the CMIP5 GCMs under RCPs (Wan et al., 2018; Satoh et al., 2021).

To the best of our knowledge, only three global studies (Cook et al., 2020; Zeng et al., 2022; Zhao and Dai, 2022) compared the expected changes in the three drought categories using the CMIP6 GCMs. However, they did not consider projection uncertainty, nor did they investigate the significance of climate change signals. More specifically, it is currently unclear how total uncertainty and its contributors as well as the signal-to-noise ratio vary among different drought types. The quantitative description of uncertainty in future drought projections and its decomposition into different contributors is essential for a better interpretation of climate change impacts for informed policy decisions and actions to mitigate the associated risk (Taylor et al., 2013; Hosseinzadehtalaei et al., 2018). The dominant source of uncertainty in climate change projections varies with climate model ensemble, variable, and region (Lehner et al., 2020; Tabari et al., 2021; Zhang and Chen, 2021). In addition to the lack of uncertainty assessments in the CMIP6 studies (Cook et al., 2020; Zeng et al., 2022; Zhao and Dai, 2022), these works did not compare different drought characteristics and did not address the full range of plausible future scenarios, which is particularly important for uncertainty analyses. We thus argue that a more systematic, comprehensive comparison of the climate change impacts on different drought types is required.

This study explores the dependency of climate change signals on drought types by comparing the spatial distribution, magnitude, and uncertainty of climate change signals for meteorological, hydrological, and agricultural droughts on a global scale. The comparison is made for five drought characteristics, i.e. median intensity, peak intensity, median duration, longest duration, and frequency, and for 3- and 12-month time scales. We characterize meteorological, hydrological, and agricultural droughts respectively by standardized precipitation index (SPI), standardized runoff index (SRI), and standardized soil moisture index (SSI) using the simulations from 18 CMIP6 GCMs for four Shared Socioeconomic Pathways (SSPs) SSP1-2.6, SSP2-4.5, SSP3-7.0, and SSP5-8.5.

## 2. Materials and methods

### 2.1. Data

To cover the traditional three categories of droughts (meteorological, agricultural, and hydrological), precipitation flux (including both liquid and solid phases), total runoff (total runoff including drainage through the base of the soil model), and total soil moisture content (water in all phases summed over all soil layers) were used. Precipitation data are analyzed only for global land grid cells to be consistent with runoff and soil moisture analysis. Though drought results may have limited practical relevance for deserts and hyper-arid regions but might be useful for a physical understanding of climate change impact. We thus performed our analyses on the entire global land area.

We used eighteen GCMs from the CMIP6 for which the concept of RCPs is integrated into ScenarioMIP and combined with SSPs. While the RCPs represent pathways towards different levels of greenhouse gas concentrations and their corresponding radiative forcing in the year 2100 (van Vuuren et al., 2011), the different SSPs describe changes in demographics, human development, economy and lifestyle, policies and institutions, technology, environment, and natural resources (O'Neill et al., 2016). The CMIP6 GCMs include ACCESS-CM2, ACCESS-ESM1-5, CAMS-CSM1-0, CanESM5, CAS-ESM2-0, CNRM-CM6-1, CNRM-ESM2-1, FGOALS-f3-L, FGOALS-g3, GFDL-ESM4, INM-CM4-8, INM-CM5-0, IPSL-CM6A-LR, MCM-UA-1-0, MIROC6, MPI-ESM1-2-HR, MPI-ESM1-2-LR, MRI-ESM2-0, all providing monthly data for precipitation, runoff, and soil moisture for historical simulations and four future tier 1 scenarios (SSP1-2.6, SSP2-4.5, SSP3-7.0, and SSP5-8.5) for the continuous period 1971–2100 (historical + SSP). These four most plausible scenarios envision different future worlds, respectively referring to the low-forcing sustainability pathway, medium-forcing middle-of-the-road pathway, medium-to high-end forcing pathway, and high-end forcing pathway.

### 2.2. Characterizing droughts

We used the SPI (McKee et al., 1993), the SRI (Shukla and Wood, 2008), and the SSI (Hao and AghaKouchak 2013) to characterize meteorological, hydrological, and agricultural droughts, respectively. These standardized indices (SPI, SRI, and SSI) were calculated for two time-scales of 3 and 12 months, representing anomalies of accumulated values for the given month and the two and eleven previous months, respectively. The anomalies were calculated for the whole period 1971–2100 as the baseline to certify a more robust quantification of the standardized index (Wu et al., 2005; Spinoni et al., 2020). Although parametric approaches to calculate the standardized indices are widely used in regional studies (Won et al., 2020; Li et al., 2020; Li et al., 2021), they have some disadvantages: 1) parametric approaches might lead to spatial sensitivity of distribution (Stagge et al., 2015; Vicente-Serrano and Beguería, 2016; Monish and Rehana, 2020; Yimer et al., 2022), 2) parametric approaches require the goodness-of-fit test and thus demand much more computation time (Dai et al., 2020), and 3) the same distribution (e.g., Gamma distribution) is hard to be applied to data across the globe under varying hydroclimatic conditions due to the limitation of the nature of distributions (Ukkola et al., 2018). To avoid the bias caused by the choice of an inappropriate distribution and massive computation time for a global study, a non-parametric distribution was used for this study (Farahmand and AghaKouchak, 2015). More specifically, we employed the Gringorten plotting position to compute the empirical probability for precipitation, runoff, and soil moisture data for each month:

$$p(x_t) = \frac{i - 0.44}{n + 0.12} \tag{1}$$

where $p(x_t)$ is the empirical probability corresponding to month $t$, $i$ is the rank of samples, and $n$ is the sample size. This probability was then standardized into SPI, SRI, and SSI values through the inverse normal transformation ($\varphi$):

$$SPI_i \,/\, SRI_i \,/\, SSI_i = \varphi^{-1}(p(x_t)) \tag{2}$$

### 2.3. Defining drought properties

After computing the SPI, SRI, and SSI time series for the period 1971–2100 for each model grid cell at a global level, the drought characteristics were determined for the historical period (1971–2000) and two future periods (2041–2070 and 2071–2100). A drought event starts when the local drought indicator is less than a threshold (−0.5 following Gu et al., 2020 and Tabari and Willems, 2022), lasts when the value is below the threshold for at least three consecutive months and ends when the index rises above the threshold. Global patterns and magnitude of changes in drought properties have shown to be similar across different thresholds (Tabari and Willems, 2022).

We define drought duration as the number of months between the start and the end of an event. The longest drought duration refers to the maximum duration in each of the historical and future periods for each pixel. Drought intensity is the average indicator value of a drought event, while drought peak intensity is the maximum drought indicator value of an event. The drought frequency is the number of drought events for the historical and future periods. After the calculation of drought characteristics, the changes were calculated as the ratio of the magnitude of drought characteristics in the future periods over that of the corresponding characteristics in the historical period. To compute the ensemble median, the changes calculated at the native resolution of the CMIP6 GCMs are resampled to a 0.5° (latitude) × 0.5° (longitude) grid. Our preliminary analyses show that the CMIP6 ensemble median results are not sensitive to the choice of the common grid size for interpolation. Due to the importance of drought intensification, we focus more on the increasing signals in the drought characteristics in the paper. The spatial extent of increasing signals for the drought characteristics is defined as the percentage of grid points with an increasing signal relative to the total land grid points.

### 2.4. Assessing sources of uncertainty

We quantified the uncertainty in the projected changes for the five characteristics of different droughts at each model grid. The uncertainty was split into GCM and SSP uncertainties. To exclude the influence of the unequal sample sizes of GCMs and SSPs on uncertainty decomposition results (Hosseinzadehtalaei et al., 2017), the variance decomposition-same sample size method (VD-SSS; Tabari et al., 2019) was used for quantifying the GCM uncertainty. Thereby the reference ensemble size was first defined as equal to the smallest sample size among uncertainty sources (four in this work). After taking the median across the four SSPs, the method then iteratively resampled the GCM ensemble by randomly selecting GCMs of the reference size (4 out of 18) and computed the standard deviation of the changes across the bootstrap samples. This process was iterated (1 000 times) and the median of the empirical bootstrap distribution of sample standard deviation was taken as the GCM uncertainty. A conventional variance decomposition method was used for quantifying the uncertainty of the source with the reference size (SSP). The total uncertainty was defined as the sum of GCM and SSP uncertainties.

The signal-to-noise (S2N) was calculated as the ratio of the ensemble median of changes to the uncertainty across the ensemble (Kendon et al., 2008). The statistical significance of S2N ratios was tested by defining a $t$-test statistic in terms of the S2N ratio following Aalbers et al. (2018). For our ensemble size (n = 18), the change is significant at the 5% level when the absolute value of S2N ratios is larger than 0.54.

## 3. Results

### 3.1. How do climate change signals differ across the characteristics of different drought types?

The future changes in different drought types for the far-future period (2071–2100) are compared in terms of five characteristics for the 12-month scale. The analysis shows that the spatial extent of increasing signals in drought intensity increases in the order of meteorological, hydrological, and agricultural drought (hereafter MET-HYD-AGR hierarchy) across all SSP scenarios (Fig. 1a–c). The percentages of the global land area with an increasing signal of drought intensity under the SSP1-2.6 scenario are 25%, 41%, and 47% for meteorological, hydrological, and agricultural droughts, respectively. For SSP5-8.5, the percentages are 33%, 47%, and 54% for the respective drought types. The MET-HYD-AGR hierarchy is also found for the intermediate scenarios (SSP2-4.5 and SSP3-7.0) and also holds for the magnitude of the increasing signals of drought intensity (Fig. 2a–c). The magnitude range across different drought types is 5–9%, 7–11%, 10–13%, and 12–13% for SSP1-2.6, SSP2-4.5, SSP3-7.0, and SSP5-8.5, respectively. Spatially, the three drought types agree on an alleviation in northern North America, central Africa, and southern Asia and on the intensification of droughts in Central America, northern South America, the Mediterranean, southern Africa, and Australia (Fig. S1). However, the sign of changes varies across different drought types in other regions.

For peak intensity, analogous regions of similarity and discrepancy across various drought types are observed, although the similarity across drought types is slightly higher for peak intensity compared to median intensity (Fig. S2). The MET-HYD-AGR hierarchy holds for both the spatial extent and magnitude of the increasing signals of peak intensity (Figs. 1 and 2). The percentage of the global land area with an increasing signal varies from 29% for meteorological drought to 46% for agricultural drought under SSP1-2.6 and from 31% for meteorological drought to 49% for agricultural drought under SSP5-8.5 (Fig. 1d–f). Compared to median intensity, the magnitude of changes is larger for peak intensity for all drought types. Following the MET-HYD-AGR hierarchy, the global median magnitude of increasing signals for peak intensity are 6%, 8%, and 12% for meteorological, hydrological, and agricultural droughts under SSP1-2.6, respectively, and 11%, 12%, and 16% for the respective scenarios under SSP5-8.5 (Fig. 2d–f).

As can clearly be seen in the results (Figs. 1 and 2), the magnitude of changes increases from intensity (average and peak) to duration (median and longest) for all drought types. Similarly, the discrepancy between various drought types grows for duration. The global median magnitudes of prolonging droughts respectively for meteorological, hydrological, and agricultural droughts are 8%, 11%, and 17% under SSP1-2.6, 11%, 13%, and 23% under SSP2-4.5, 15%, 19%, and 29% under SSP3-7.0, and 18%, 20%, and 32% under SSP5-8.5 (Fig. 2g–i). The percentage of spatial discrepancy across the results of different drought types is similar between peak intensity and median duration. The spatial-extent discrepancy for median duration resembles that of peak intensity (Fig. S3). The discrepancy in the sign of changes is seen in 16–17% of the global land for median duration, which is close to 17–18% for peak intensity and lower than 19–22% for median intensity. The proportion of the land with an increasing signal of duration varies across the three drought types within the range of 24–39% for SSP1 and 25–42% for SSP5-8.5 (Fig. 1g–i).

In terms of magnitude, the largest discrepancy among the three drought types is seen for longest drought duration (Fig. 2). The regions with the greatest differences are primarily located in Europe and Central America (Fig. 3, S6-8). The global median magnitudes of increasing signals for longest drought duration respectively for SSP1-2.6, SSP2-4.5, SSP3-7.0, and SSP5-8.5 are 11%, 14%, 21%, and 26% for meteorological drought which rise to 25%, 33%, 41%, and 44% for the respective SSPs for agricultural drought (Fig. 2j-l). The spatial discrepancy between drought types for the sign of the changes in longest duration bears a resemblance to median duration (Fig. S4), albeit the discrepancy rate is slightly larger for the former (16–19% vs. 16–17%) (Fig. 2).

Among the drought characteristics, the largest discrepancy in the spatial pattern of changes across the three drought types concerns the

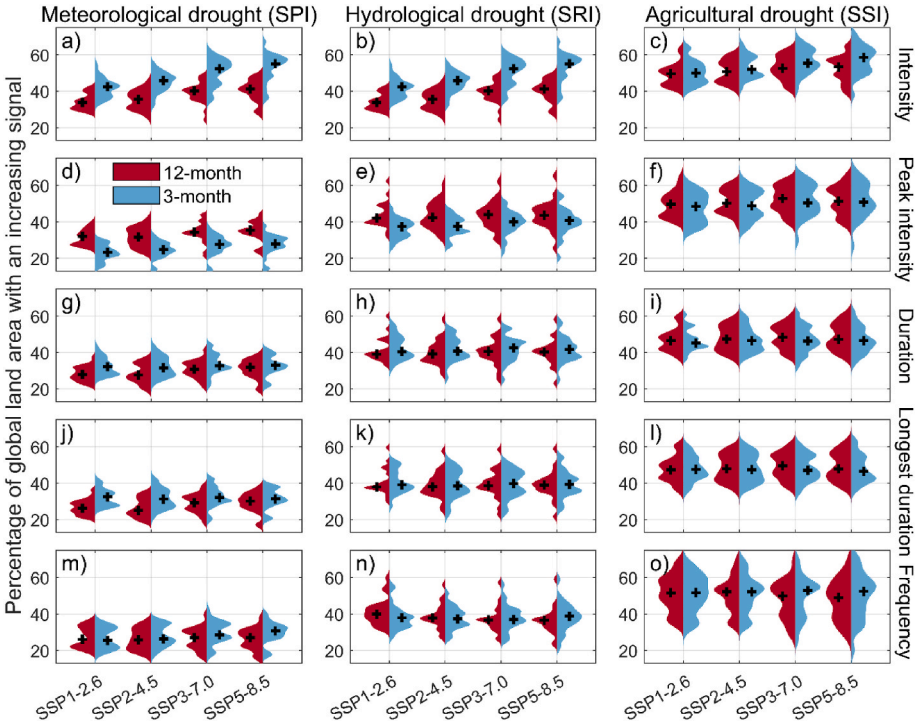


**Fig. 1.** Comparison of the spatial extent of the increasing signals in different characteristics (row) of three drought types (column) under different SSP scenarios between annual (12-month) and seasonal (3-month) scales. Violin plots depict ensemble probability density, and the ensemble median is shown by black cross. The changes are computed by comparing the characteristics between the historical (1971–2000) to the far-future (2071–2100) periods.

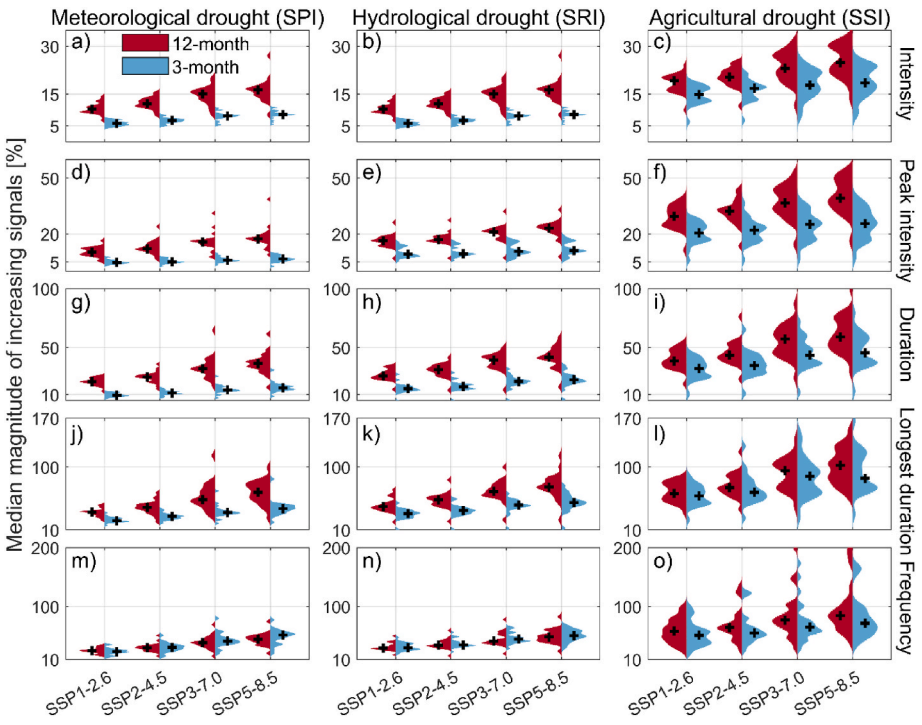


**Fig. 2.** Comparison of the median magnitude of the increasing signals in different characteristics (row) of three drought types (column) under different SSP scenarios between annual (12-month) and seasonal (3-month) scales. Violin plots depict ensemble probability density, and the ensemble median is shown by black cross. The changes are computed by comparing the characteristics between the historical (1971–2000) to the far-future (2071–2100) periods. Due to a large difference of the magnitude of the increasing signals between different characteristics, for a better visibility of the results, individual y-axis limits are selected for each characteristic.

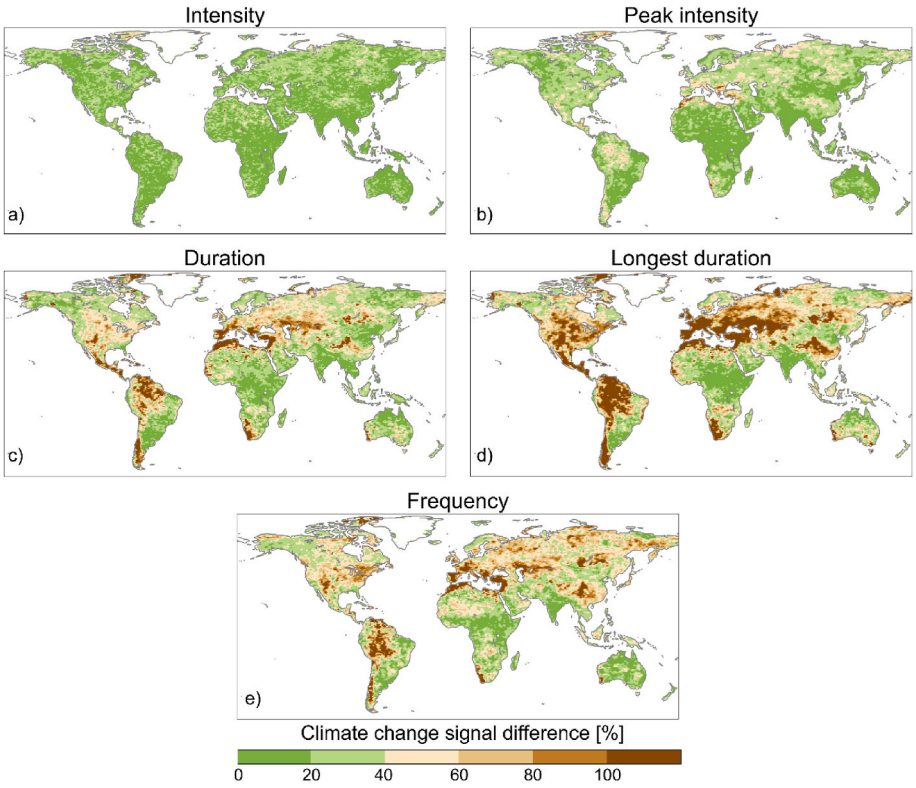


**Fig. 3.** Relative change differences (statistical range; largest value minus smallest value) among the three drought types for different characteristics at an annual (12-month) scale, under the SSP5-8.5 scenario. The relative changes were computed between the historical (1971–2000) and the far-future (2071–2100) periods. The results are based on the ensemble median of 18 CMIP6 GCMs.

drought frequency (Fig. S5), which reaches 32% between meteorological and agricultural droughts. In contrast to the other drought characteristics, the spatial extent of increasing signals for drought frequency declines with SSP scenarios, which is more noticeable for agricultural and hydrological droughts (Fig. 1m-o). It implies that drought duration increases with SSP scenarios for the benefit of a decrease in frequency. The spatial extent of increasing drought frequency across the drought types declines from 25 to 57% for SSP1-2.6 to 24–40% for SSP5-8.5. The

difference in the magnitude of increasing signals for frequency is smaller than that of duration (median and longest) but larger than intensity (median and peak). Following the MET-HYD-AGR hierarchy, the global median magnitudes of increasing signals for frequency are 10%, 13%, and 18% under SSP1-2.6 and 17%, 22%, and 26% under SSP5-8.5 (Fig. 2m-o).

In terms of the magnitude of increasing signals, the drought types show the largest discrepancy for drought duration (median and longest). The drought characteristics in ascending order of discrepancy between the magnitude of increasing signals across the three drought types are intensity, peak intensity, frequency, duration, and longest duration (Fig. 3, S6-8). There are different patterns for the discrepancy in the spatial extent of increasing signals: large differences are found between the spatial extent of increasing signals across different drought types for frequency and intensity and small differences for duration (Figs. 1 and 2).

In order to explore the sensitivity of the differences between the results of various drought types to the time scale, the results for the 3- and 12-month scales are compared (Figs. 1 and 2). For all drought characteristics, the sensitivity of the differences to the time scale is much larger for the magnitude of increasing signals compared with its spatial extent. For drought intensity, the differences in the spatial extent of increasing signals become larger with the time scale by 24%, while they become smaller with the time scale by 29% for the magnitude of increasing signals. This is because the spatial extent of intensifying droughts decreases with the time scale at a higher rate for meteorological drought (23%) compared with hydrological (11%) and agricultural (4%) droughts. A similar pattern but in the opposite order is found for the magnitude of intensifying droughts where it increases with the time scale at a higher rate for meteorological drought (82%) compared with hydrological (56%) and agricultural (28%) droughts.

For peak intensity, the differences between the results of various drought types decrease with the time scale by 20% and 40% for the spatial extent and magnitude of increasing signals, respectively. Similar to intensity, the discrepancy among drought types for duration enlarges for the spatial extent (13% for median duration and 18% for longest duration) and reduces for the magnitude (44% for median duration and 26% for longest duration). For frequency, while the discrepancy for the spatial extent remains almost the same by changing the time scale because of minor changes in peak values from the 12-month to 3-month scale, it increases by 22% for the magnitude of increasing signals.

Climate change signals of different drought types were compared for the mid-future period (2041–2070), and the MET-HYD-AGR hierarchy is found to hold for this period as well. The areas with large differences among the various drought types are similar to those observed in the far-future period (2071–2 100) (Figs. S9–S12).

### 3.2. How do projection uncertainties and signal-to-noise ratios differ across different drought types?

Along with climate change signals, the uncertainty in the projections of all the drought characteristics for the far-future period (2071–2 100) at both 3- and 12-month scales also increases from meteorological to hydrological to agricultural drought (Fig. 4a and b). The total uncertainty for median intensity, peak intensity, median duration, longest duration, and frequency of agricultural drought is respectively 4.7, 4.9, 1.4, 7.2, and 5.4 times larger than that of meteorological drought for the 3-month scale. For the 12-month scale, the total uncertainty for the respective characteristics of agricultural drought is 3.3, 3.7, 1.4, 2.3, and 3 times larger than that of meteorological drought. As previously reported (Lehner et al., 2020), climate change uncertainty increases with lead time toward the end of the 21st century (Fig. S13). However, the MET-HYD-AGR hierarchy for the uncertainty of drought projections in the far-future period holds for the mid-future period.

The decomposition of the total uncertainty into GCM and SSP sources shows that for all three drought types the GCM uncertainty is the dominant source for all five characteristics and for two time scales (Fig. 4c and d). Depending on drought types and characteristics, GCM differences explain 68–84% of the total variance in climate change signals for the 3-month scale and 66–82% for the 12-month scale. Both GCM and SSP uncertainties also increase from meteorological to hydrological to agricultural drought. Since this increase is larger for GCM-related uncertainty compared to those of SSPs for all characteristics (except peak intensity at the 3-month scale), the fractional contribution of GCM-related uncertainty follows the MET-HYD-AGR hierarchy while that of SSPs is the opposite.

The spatial distribution of the GCM uncertainty differences among the three drought types for the far-future period reveals that the global medians of the differences are 9%, 16%, 21%, 34%, and 39% respectively for intensity, peak intensity, duration, longest duration, and frequency (Fig. 5). The GCM uncertainty difference is not globally uniform. For all drought characteristics, the GCM uncertainty differences between the three drought types are larger in the Northern Hemisphere compared to the Southern Hemisphere, and the lowest differences are present in central Africa and southern and eastern Asia. The GCM uncertainty difference for intensity is less than 20% for almost the entire

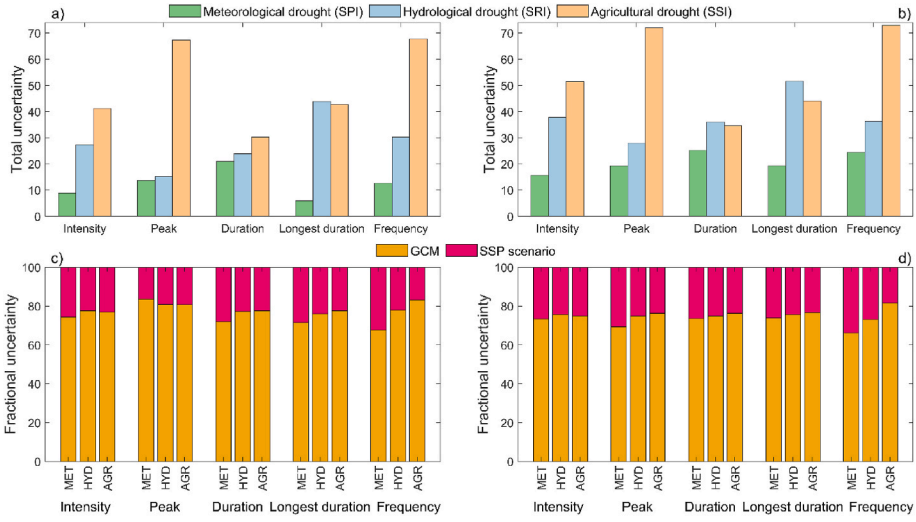


**Fig. 4.** Total (a, b) and fractional (c, d) uncertainties for changes in different drought types at the times scales of 3 (a, c) and 12 months (b, d) for the far-future period (2071–2100).

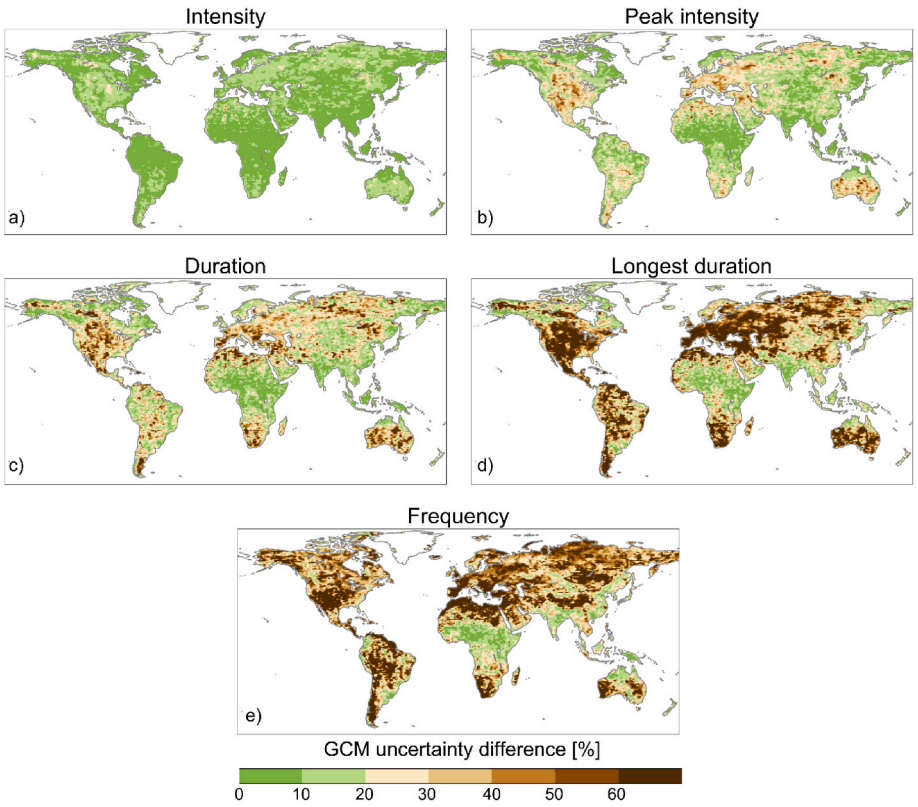


**Fig. 5.** GCM uncertainty differences (statistical range; largest value minus smallest value) among the three drought types for different characteristics for the far-future period (2071–2100).

world. While the GCM uncertainty difference of >50% is found in <10% of the global land area for peak intensity and duration, it exceeds 30% of the land for longest duration and frequency.

The increase of both signal and noise (uncertainty) from meteorological to hydrological to agricultural drought raises the question of how the signal-to-noise ratios (S2N) would change between the three drought types. Our results indicate that the MET-HYD-AGR hierarchy holds for the spatial extent of significant S2N for all drought characteristics except frequency (Fig. 6). It implies a more important role of climate change signals than uncertainty for the spatial distribution of droughts. For

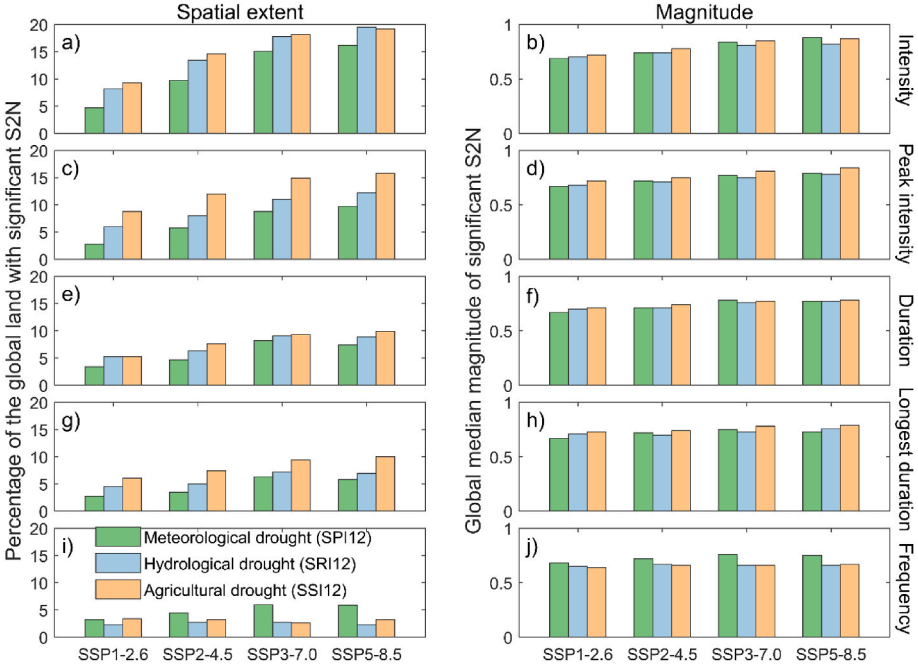


**Fig. 6.** Comparison of the spatial extent (left column) and magnitude (right column) of significant signal-to-noise ratios (S2N) in different characteristics (row) of three drought types under different SSP scenarios based on the ensemble median of 18 CMIP6 GCMs. The increases from the historical period (1971–2000) to the far-future (2071–2100) period at the annual (12-month) scale are shown.

increasing signals, a significant S2N ratio for drought intensity under SSP1-2.6 is found in 5% of the global land area for meteorological drought, 8% for hydrological drought, and 9% for agricultural drought. The percentages of the land with a significant S2N of intensity for SSP5-8.5 grows to 16%, 16%, and 19% for the respective drought types. The percentages for the intermediate scenarios (SSP2-4.5and SSP3-7.0) are within the range of the extreme scenarios (SSP1-2.6 and SSP5-8.5). Similarly, for increasing peak intensity, the percentage of the land with a significant S2N increases from 3 to 10%, depending on the SSP scenarios, for meteorological drought to 9–16% for agricultural drought. A significant S2N for prolonging duration is seen in 3–7%, 5–9%, and 5–10% of the global land for meteorological, hydrological, and agricultural droughts, respectively. A similar spatial extent of significant S2N is found for longest duration, accounting for 3–6% for meteorological drought, 5–7% for hydrological drought, and 6–10% for agricultural drought. Among all the characteristics, frequency shows a different pattern. In contrast to the spatial extent of significant S2N, its magnitude is similar across different drought types. The MET-HYD-AGR hierarchy for S2N also holds for the mid-future period (Fig. S14).

The largest S2N discrepancy among drought types is found in the Northern Hemisphere, especially where a decreasing signal of meteorological drought is projected (Fig. 7, S15-S17). For all drought characteristics, the S2N discrepancy increases with the SSP scenarios. For SSP5-8.5, the global medians of the S2N difference are 76%, 74%, 99%, 107%, and 90% for median intensity, peak intensity, median duration, longest duration, and frequency, respectively. The global medians of the S2N difference decrease to 64%, 57%, 80%, 89%, and 71% for the respective characteristics under SSP1-2.6.

## 4. Discussion

The results of this study highlight the increasing climate change signals from meteorological to hydrological to agricultural drought, where the characteristics of agricultural drought show, on average, twice as large an increase in spatial extent and magnitude compared to meteorological drought. Precipitation shortage can be strengthened through a positive loop feedback where dry soil and reduced vegetation cover would increase the surface albedo, limit evapotranspiration, and increase surface warming, thereby intensifying meteorological drought (Taylor et al., 2002; Dai et al., 2018). The changes in soil moisture and runoff are mainly driven by the changes in precipitation and evapotranspiration (Zhao and Dai, 2015, 2022). The projected ubiquitous increase in evapotranspiration (Tabari et al., 2021), which is missing in meteorological drought, reinforces precipitation decreases in some regions and offsets precipitation increases in other regions, while increased runoff can offset soil moisture increases due to increased precipitation (Zhao and Dai, 2022).

The changes in all the characteristics of meteorological and hydrological droughts are consistent in the Southern Hemisphere. However, opposite changes are found in some regions in the Northern Hemisphere such as North America, Europe, and central Asia. These are mostly snow-dominated regions where snow dynamics are important. In these regions, global warming induced changes in snowmelt timing (Musselman et al., 2017), snow water equivalent (SWE; Shi and Wang, 2015), and snow-rain partitioning (Burn and Whitfield, 2016) play central roles. Similarly, flood changes in these regions would not follow the changes in extreme precipitation due to the role of snow dynamics (Tabari, 2021).

Similar to climate change signals, total uncertainty also increases from meteorological to hydrological to agricultural drought. This enlarging pattern is observed for both GCM and SSP uncertainties. The enlargement of GCM uncertainty is due to the increasing complexity from precipitation to runoff to soil moisture to be modeled by GCMs. This complexity is evident from the larger bias of surface runoff and soil moisture simulations compared to precipitation in CMIP6 GCMs (Qiao et al., 2022). As models struggle to accurately represent hydrological and agricultural droughts and their related mechanisms, a large uncertainty is expected in future projections due to the different representations of these mechanisms by GCMs. In fact, runoff and soil moisture

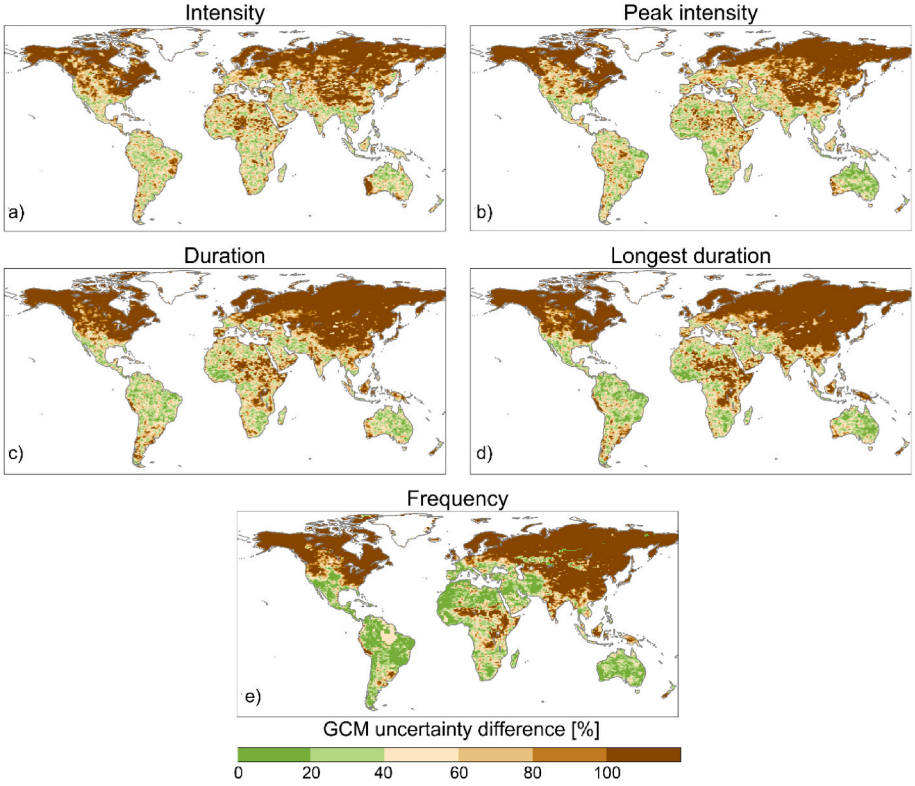


**Fig. 7.** Signal-to-noise ratio differences (statistical range; largest value minus smallest value) among the three drought types for different characteristics under the SSP5-8.5 scenario for the far-future period (2071–2100).

projections inherit the uncertainty associated with precipitation (i.e., error propagation) next to their own uncertainties arising from different representations of hydrological processes by GCMs (Lu et al., 2019). To accurately project future soil moisture, a variety of factors must be considered, such as future precipitation under warming, sophisticated hydrological processes, land surface changes, wind speed, and atmospheric CO2 (Sheffield and Wood, 2008). However, many CMIP6 GCMs employ simplified hydrological models that omit complex treatments of certain hydrological processes (Mueller and Seneviratne, 2014), leading to greater uncertainties in modeled soil moisture. Some of the hydrological processes that have been omitted include lateral groundwater flow, lateral flow of reinfiltrating river water, and irrigation with river water (Zampieri et al., 2012; Greve et al., 2014; Clark et al., 2015). Additionally, the highly variable data output among different models is due to the employment of various structures and physical parameterization schemes (Gleckler et al., 2008; Jamison and Kravtsov 2010). The representation of snow cover and its links with climate in LSMs is a known source of bias in runoff and soil moisture simulations of climate models. To ensure accurate capturing of the timing and atmospheric response to snowmelt in climate models, it's important to consider the temporal dynamics of snow-atmospheric coupling throughout different stages of snow depletion (Xu and Dirmeyer, 2011, 2012). Snow-albedo feedback, the energy sink caused by spring snow melting, and the thermal insulation effect of snow on the underlying soil are all factors that can lead to biases in climate models related to snow (Koven et al., 2013; Gouttevin et al., 2012; Bart Van den Hurk et al., 2016). LSMs were found to be an important source of GCM uncertainty in historical CMIP5 runoff and soil moisture drought simulations (Ukkola et al., 2018). A lower GCM uncertainty for the average drought duration and intensity of meteorological drought compared to those of hydrological and agricultural droughts for historical periods was partly attributed to the shorter duration of meteorological droughts (Ukkola et al., 2018).

## 5. Conclusions

This work compared climate change signals and signal-to-noise ratios for five drought characteristics between meteorological, hydrological, and agricultural droughts at the global scale using CMIP6 GCM simulations. The results show that the spatial distribution and magnitude of increasing signals in all five drought characteristics rise from meteorological to hydrological to agricultural drought. Similarly, uncertainty increases from meteorological to hydrological to agricultural drought. Despite this uncertainty enlargement, the MET-HYD-AGR hierarchy holds for the spatial extent of significant signal-to-noise ratios for all drought characteristics except frequency. The magnitude of significant S2N, however, revealed a mixed pattern.

Our results show that precipitation drought cannot substitute as proxies for runoff and soil moisture droughts because of their spatially-varying responses to climate change, different uncertainties, and signal-to-noise ratios. The difference in the results of different drought types is particularly pronounced in regions where opposite signs of changes and very different levels of confidence (in terms of signal-to-noise ratios) are found. Particular care is required when using drought indicators for different drought categories, e.g., use of precipitation drought for analyzing the vulnerability of crop production to droughts (Kim et al., 2019; Leng and Hall, 2019), which might lead to inadequately-targeted mitigation and adaptation strategies. Larger uncertainties of runoff and soil moisture droughts highlight the need for a better understanding of the key processes governing runoff and soil moisture droughts and their representations in land-surface models, although these might not necessarily lead to reduced uncertainties in the projections. Our study compared drought types based on their hazards, but recent studies have shown that exposure and vulnerability play significant roles in shaping future drought risks (Tabari et al., 2021). Therefore, future research can compare drought types based on impacts such as exposed population or assets, as done in recent studies (Spinoni et al., 2021; Yin et al., 2023).

## Author statement

Parisa Hosseinzadehtalaei: Conceptualization, Methodology, Software, Formal analysis, Writing - Original Draft, Review & Editing, Visualization. Bert Van Schaeybroeck: Writing - Review & Editing. Piet Termonia: Writing - Review & Editing, Supervision. Hossein Tabari: Conceptualization, Methodology, Writing - Review & Editing, Supervision.

## Declaration of competing interest

The authors declare that they have no known competing financial interests or personal relationships that could have appeared to influence the work reported in this paper.

## Data availability

All the data used in this paper are publicly available.

## Acknowledgments

The first author wishes to express her appreciation to the Research Foundation – Flanders (FWO) for funding this work (grant number: 1255423N). The CMIP6 data providers are also acknowledged. The CMIP6 soil moisture, runoff and precipitation data used in this study can be accessed online through the Earth System Grid Federation (ESGF) system.

## Appendix A. Supplementary data

Supplementary data to this article can be found online at https://doi.org/10.1016/j.wace.2023.100573.

## References

Ahmadalipour, A., Moradkhani, H., Castelletti, A., Magliocca, N., 2019. Future drought risk in Africa: integrating vulnerability, climate change, and population growth. Sci. Total Environ. 662, 672–686.
Arora, V.K., Seiler, C., Wang, L., Kou-Giesbrecht, S., 2023. Towards an ensemble-based evaluation of land surface models in light of uncertain forcings and observations. Biogeosciences 20 (7), 1313–1355.
Berg, A., Sheffield, J., 2018. Climate change and drought: the soil moisture perspective. Curr. Clim. Change Rep. 4 (2), 180–191.
Berg, A., Sheffield, J., Milly, P.C., 2017. Divergent surface and total soil moisture projections under global warming. Geophys. Res. Lett. 44 (1), 236–244.
Burn, D.H., Whitfield, P.H., 2016. Changes in floods and flood regimes in Canada. Can. Water Resour. J. 41 (1–2), 139–150.
Burke, E.J., Brown, S.J., 2008. Evaluating uncertainties in the projection of future drought. J. Hydrometeorol. 9 (2), 292–299.
Chen, X., Tian, F., Su, Y., 2022. How did the late 1920s drought affect northern Chinese society? Weather Clim. Extrem. 36, 100451.
Chiang, F., Mazdiyasni, O., AghaKouchak, A., 2021. Evidence of anthropogenic impacts on global drought frequency, duration, and intensity. Nat. Commun. 12 (1), 1–10.
Clark, M.P., Fan, Y., Lawrence, D.M., Adam, J.C., Bolster, D., Gochis, D.J., et al., 2015. Improving the representation of hydrologic processes in Earth system models. Water Resour. Res. 51 (8), 5929–5956.
Coppola, E., et al., 2021. Climate hazard indices projections based on CORDEX-CORE, CMIP5 and CMIP6 ensemble. Clim. Dynam. 57, 1293–1383.
Cook, B.I., Mankin, J.S., Anchukaitis, K.J., 2018. Climate change and drought: from past to future. Curr. Clim. Change Rep. 4 (2), 164–179.
Cook, B.I., Mankin, J.S., Marvel, K., Williams, A.P., Smerdon, J.E., Anchukaitis, K.J., 2020. Twenty-first century drought projections in the CMIP6 forcing scenarios. Earth's Future 8 (6), e2019EF001461.
Dai, A., Zhao, T., Chen, J., 2018. Climate change and drought: a precipitation and evaporation perspective. Curr. Clim. Change Rep. 4 (3), 301–312.
Dai, C., Qin, X.S., Lu, W.T., Zang, H.K., 2020. A multimodel assessment of drought characteristics and risks over the Huang-Huai-Hai River basin, China, under climate change. Theor. Appl. Climatol. 141 (1), 601–613.
Eyring, V., Bony, S., Meehl, G.A., Senior, C.A., Stevens, B., Stouffer, R.J., Taylor, K.E., 2016. Overview of the coupled model intercomparison project phase 6 (CMIP6) experimental design and organization. Geosci. Model Dev. (GMD) 9 (5), 1937–1958.
Eyring, V., Cox, P.M., Flato, G.M., Gleckler, P.J., Abramowitz, G., Caldwell, P., et al., 2019. Taking climate model evaluation to the next level. Nat. Clim. Change 9 (2), 102–110.

Farahmand, A., AghaKouchak, A., 2015. A generalized framework for deriving nonparametric standardized drought indicators. Adv. Water Resour. 76, 140–145.
Fisher, R.A., Koven, C.D., 2020. Perspectives on the future of land surface models and the challenges of representing complex terrestrial systems. J. Adv. Model. Earth Syst. 12 (4), e2018MS001453.
Gleckler, P.J., Taylor, K.E., Doutriaux, C., 2008. Performance metrics for climate models. J. Geophys. Res. Atmos. 113 (D6) https://doi.org/10.1029/2007JD008972.
Gouttevin, I., Menegoz, M., Dominé, F., Krinner, G., Koven, C., Ciais, P., et al., 2012. How the insulating properties of snow affect soil carbon distribution in the continental pan-Arctic area. J. Geophys. Res.: Biogeosciences 117 (G2). https://doi.org/10.1029/2011JG001916.
Greve, P., Orlowsky, B., Mueller, B., Sheffield, J., Reichstein, M., Seneviratne, S.I., 2014. Global assessment of trends in wetting and drying over land. Nat. Geosci. 7 (10), 716–721.
Gu, L., Chen, J., Yin, J., Sullivan, S.C., Wang, H.M., Guo, S., Kim, J.S., 2020. Projected increases in magnitude and socioeconomic exposure<? xmltex\break?> of global droughts in 1.5 and 2◦ C warmer climates. Hydrol. Earth Sys. Sci. 24 (1), 451–472.
Hao, Z., AghaKouchak, A., 2013. Multivariate standardized drought index: a parametric multi-index model. Adv. Water Resour. 57, 12–18.
Hosseinzadehtalaei, P., Tabari, H., Willems, P., 2017. Uncertainty assessment for climate change impact on intense precipitation: how many model runs do we need? Int. J. Climatol. 37, 1105–1117.
Hosseinzadehtalaei, P., Tabari, H., Willems, P., 2018. Precipitation intensity–duration–frequency curves for central Belgium with an ensemble of EURO-CORDEX simulations, and associated uncertainties. Atmos. Res. 200, 1–12.
IPCC, 2022. In: Portner,¨H.-O (Ed.), Climate Change 2022: Impacts, Adaptation, and Vulnerability, Contribution of Working Group II to the Sixth Assessment Report of the Intergovernmental Panel on Climate Change. Cambridge University Press.
Jamison, N., Kravtsov, S., 2010. Decadal variations of North Atlantic sea surface temperature in observations and CMIP3 simulations. J. Clim. 23 (17), 4619–4636.
Ji, Y., Li, Y., Yao, N., Biswas, A., Chen, X., Li, L., et al., 2022. Multivariate global agricultural drought frequency analysis using kernel density estimation. Ecol. Eng. 177, 106550.
Joo, J., Jeong, S., Zheng, C., Park, C.E., Park, H., Kim, H., 2020. Emergence of significant soil moisture depletion in the near future. Environ. Res. Lett. 15 (12), 124048.
Kendon, E.J., Rowell, D.P., Jones, R.G., Buonomo, E., 2008. Robustness of future changes in local precipitation extremes. J. Clim. 21 (17), 4280–4297.
Kim, W., Iizumi, T., Nishimori, M., 2019. Global patterns of crop production losses associated with droughts from 1983 to 2009. J. Appl. Meteorol. Climatol. 58 (6), 1233–1244.
Koven, C.D., Riley, W.J., Stern, A., 2013. Analysis of permafrost thermal dynamics and response to climate change in the CMIP5 Earth System Models. J. Clim. 26 (6), 1877–1900.
Lauenroth, W.K., Schlaepfer, D.R., Bradford, J.B., 2014. Ecohydrology of dry regions: storage versus pulse soil water dynamics. Ecosystems 17 (8), 1469–1479.
Lehner, F., Deser, C., Maher, N., Marotzke, J., Fischer, E.M., Brunner, L., et al., 2020. Partitioning climate projection uncertainty with multiple large ensembles and CMIP5/6. Earth System Dynamics 11 (2), 491–508.
Leng, G., Hall, J., 2019. Crop yield sensitivity of global major agricultural countries to droughts and the projected changes in the future. Sci. Total Environ. 654, 811–821.
Li, H., Li, Z., Chen, Y., Xiang, Y., Liu, Y., Kayumba, P.M., Li, X., 2021. Drylands face potential threat of robust drought in the CMIP6 SSPs scenarios. Environ. Res. Lett. 16 (11), 114004.
Li, L., She, D., Zheng, H., Lin, P., Yang, Z.L., 2020. Elucidating diverse drought characteristics from two meteorological drought indices (SPI and SPEI) in China. J. Hydrometeorol. 21 (7), 1513–1530.
Lu, J., Carbone, G.J., Grego, J.M., 2019. Uncertainty and hotspots in 21st century projections of agricultural drought from CMIP5 models. Sci. Rep. 9 (1), 1–12.
Mankin, J.S., Seager, R., Smerdon, J.E., Cook, B.I., Williams, A.P., 2019. Mid-latitude freshwater availability reduced by projected vegetation responses to climate change. Nat. Geosci. 12 (12), 983–988.
McKee, T.B., Doesken, N.J., Kleist, J., 1993. The relationship of drought frequency and duration to time scale (Anaheim, CA, 17–22 January) 8th Conf. Appl. Climatol.
Milly, P.C., Dunne, K.A., 2016. Potential evapotranspiration and continental drying. Nat. Clim. Change 6 (10), 946–949.
Monish, N.T., Rehana, S., 2020. Suitability of distributions for standard precipitation and evapotranspiration index over meteorologically homogeneous zones of India. J. Earth Syst. Sci. 129 (1), 1–19.
Mueller, B., Seneviratne, S.I., 2014. Systematic land climate and evapotranspiration biases in CMIP5 simulations. Geophys. Res. Lett. 41 (1), 128–134.
Musselman, K.N., Clark, M.P., Liu, C., Ikeda, K., Rasmussen, R., 2017. Slower snowmelt in a warmer world. Nat. Clim. Change 7 (3), 214–219.
O'Neill, B.C., et al., 2016. The scenario model intercomparison project (ScenarioMIP) for CMIP6. Geosci. Model Dev. (GMD) 9 (9), 3461–3482.
Orlowsky, B., Seneviratne, S.I., 2013. Elusive drought: uncertainty in observed trends and short-and long-term CMIP5 projections. Hydrol. Earth Syst. Sci. 17 (5), 1765–1781.
Pokhrel, Y., Felfelani, F., Satoh, Y., Boulange, J., Burek, P., Gädeke, A., et al., 2021. Global terrestrial water storage and drought severity under climate change. Nat. Clim. Change 11 (3), 226–233.
Prudhomme, C., Giuntoli, I., Robinson, E.L., Clark, D.B., Arnell, N.W., Dankers, R., et al., 2014. Hydrological droughts in the 21st century, hotspots and uncertainties from a global multimodel ensemble experiment. Proc. Natl. Acad. Sci. USA 111 (9), 3262–3267.
Qiao, L., Zuo, Z., Xiao, D., 2022. Evaluation of soil moisture in CMIP6 simulations. J. Clim. 35 (2), 779–800.
Satoh, Y., Shiogama, H., Hanasaki, N., Pokhrel, Y., Boulange, J.E.S., Burek, P., et al., 2021. A quantitative evaluation of the issue of drought definition: a source of disagreement in future drought assessments. Environ. Res. Lett. 16 (10), 104001.
Schlaepfer, D.R., Bradford, J.B., Lauenroth, W.K., Munson, S.M., Tietjen, B., Hall, S.A., et al., 2017. Climate change reduces extent of temperate drylands and intensifies drought in deep soils. Nat. Commun. 8 (1), 1–9.
Séférian, R., Nabat, P., Michou, M., Saint-Martin, D., Voldoire, A., Colin, J., et al., 2019. Evaluation of CNRM Earth System Model, CNRM-ESM2-1: role of Earth system processes in present-day and future climate. J. Adv. Model. Earth Syst. 11 (12), 4182–4227.
Shi, H.X., Wang, C.H., 2015. Projected 21st century changes in snow water equivalent over Northern Hemisphere landmasses from the CMIP5 model ensemble. Cryosphere 9 (5), 1943–1953.
Shukla, S., Wood, A.W., 2008. Use of a standardized runoff index for characterizing hydrologic drought. Geophys. Res. Lett. 35 (2).
Spinoni, J., et al., 2020. Future global meteorological drought hot spots: a study based on CORDEX Data. J. Clim. 33 (9), 3635–3661.
Spinoni, J., et al., 2021. Global exposure of population and land-use to meteorological droughts under different warming levels and SSPs: a CORDEX-based study. Int. J. Climatol. 41 (15), 6825–6853.
Stagge, J.H., Tallaksen, L.M., Gudmundsson, L., Van Loon, A.F., Stahl, K., 2015. Candidate distributions for climatological drought indices (SPI and SPEI). Int. J. Climatol. 35 (13), 4027–4040.
Strebel, L., Bogena, H.R., Vereecken, H., Hendricks Franssen, H.J., 2022. Coupling the Community Land Model version 5.0 to the parallel data assimilation framework PDAF: description and applications. Geosci. Model Dev. (GMD) 15 (2), 395–411.
Tabari, H., 2021. Extreme value analysis dilemma for climate change impact assessment on global flood and extreme precipitation. J. Hydrol. 593, 125932.
Tabari, H., Willems, P., 2018. More prolonged droughts by the end of the century in the Middle East. Environ. Res. Lett. 13 (10), 104005.
Tabari, H., Willems, P., 2022. Trivariate analysis of changes in drought characteristics in the CMIP6 multi-model ensemble at global warming levels of 1.5, 2 and 3° C. J. Clim. 35, 5823–5837.
Tabari, H., Hosseinzadehtalaei, P., AghaKouchak, A., Willems, P., 2019. Latitudinal heterogeneity and hotspots of uncertainty in projected extreme precipitation. Environ. Res. Lett. 14 (12), 124032.
Tabari, H., Hosseinzadehtalaei, P., Thiery, W., Willems, P., 2021. Amplified drought and flood risk under future socioeconomic and climatic change. Earth's Future 9 (10), e2021EF002295.
Taylor, C.M., Lambin, E.F., Stephenne, N., Harding, R.J., Essery, R.L., 2002. The influence of land use change on climate in the Sahel. J. Clim. 15 (24), 3615–3629.
Taylor, I.H., Burke, E., McColl, L., Falloon, P.D., Harris, G.R., McNeall, D., 2013. The impact of climate mitigation on projections of future drought. Hydrol. Earth Syst. Sci. 17 (6), 2339–2358.
Touma, D., Ashfaq, M., Nayak, M.A., Kao, S.C., Diffenbaugh, N.S., 2015. A multi-model and multi-index evaluation of drought characteristics in the 21st century. J. Hydrol. 526, 196–207.
Ukkola, A.M., De Kauwe, M.G., Roderick, M.L., Abramowitz, G., Pitman, A.J., 2020. Robust future changes in meteorological drought in CMIP6 projections despite uncertainty in precipitation. Geophys. Res. Lett. 47 (11), e2020GL087820.
Ukkola, A.M., Pitman, A.J., De Kauwe, M.G., Abramowitz, G., Herger, N., Evans, J.P., Decker, M., 2018. Evaluating CMIP5 model agreement for multiple drought metrics. J. Hydrometeorol. 19 (6), 969–988.
Van den Hurk, B., Kim, H., Krinner, G., Seneviratne, S.I., Derksen, C., Oki, T., et al., 2016. LS3MIP (v1. 0) contribution to CMIP6: the Land Surface, Snow and Soil moisture Model Intercomparison Project–aims, setup and expected outcome. Geosci. Model Dev. (GMD) 9 (8), 2809–2832.
van der Wiel, K., Lenderink, G., de Vries, H., 2021. Physical storylines of future European drought events like 2018 based on ensemble climate modelling. Weather Clim. Extrem. 33, 100350.
Van Vuuren, D.P., et al., 2011. The representative concentration pathways: an overview. Climatic Change 109 (1), 5–31.
Vicente-Serrano, S.M., Beguería, S., 2016. Comment on 'Candidate distributions for climatological drought indices (SPI and SPEI)'by James H. Stagge et al. Int. J. Climatol. 36 (4), 2120–2131.
Vicente-Serrano, S.M., Domínguez-Castro, F., McVicar, T.R., Tomas-Burguera, M., Peña-Gallardo, M., Noguera, I., et al., 2020. Global characterization of hydrological and meteorological droughts under future climate change: the importance of timescales, vegetation-CO2 feedbacks and changes to distribution functions. Int. J. Climatol. 40 (5), 2557–2567.
Wan, W., Zhao, J., Li, H.Y., Mishra, A., Hejazi, M., Lu, H., et al., 2018. A holistic view of water management impacts on future droughts: a global multimodel analysis. J. Geophys. Res. Atmos. 123 (11), 5947–5972.
Wanders, N., Wada, Y., 2015. Human and climate impacts on the 21st century hydrological drought. J. Hydrol. 526, 208–220.
Wang, T., Tu, X., Singh, V.P., Chen, X., Lin, K., 2021. Global data assessment and analysis of drought characteristics based on CMIP6. J. Hydrol. 596, 126091.
Wartenburger, R., Hirschi, M., Donat, M.G., Greve, P., Pitman, A.J., Seneviratne, S.I., 2017. Changes in regional climate extremes as a function of global mean temperature: an interactive plotting framework. Geosci. Model Dev. (GMD) 10 (9), 3609–3634.
Won, J., Choi, J., Lee, O., Kim, S., 2020. Copula-based Joint Drought Index using SPI and EDDI and its application to climate change. Sci. Total Environ. 744, 140701.
Wu, H., Hayes, M.J., Wilhite, D.A., Svoboda, M.D., 2005. The effect of the length of record on the standardized precipitation index calculation. Int. J. Climatol. 25, 505–520.

Xu, L., Dirmeyer, P., 2011. Snow-atmosphere coupling strength in a global atmospheric model. Geophys. Res. Lett. 38 (13) https://doi.org/10.1029/2011GL048049.
Yimer, E.A., Van Schaeybroeck, B., Van de Vyver, H., van Griensven, A., 2022. Evaluating probability distribution functions for the standardized precipitation evapotranspiration index over Ethiopia. Atmosphere 13 (2022), 364.
Yin, J., et al., 2023. Future socio-ecosystem productivity threatened by compound drought–heatwave events. Nat. Sustain. 6, 259–272.
Yuan, S., Quiring, S.M., Leasor, Z.T., 2021. Historical changes in surface soil moisture over the contiguous United States: an assessment of CMIP6. Geophys. Res. Lett. 48 (1), e2020GL089991.
Zachariah, M., Kumari, S., Mondal, A., Haustein, K., Otto, F.E., 2022. Attribution of the 2015 Drought in Marathwada, India from a Multivariate Perspective. Weather and Climate Extremes, 100546.
Zampieri, M., Serpetzoglou, E., Anagnostou, E.N., Nikolopoulos, E.I., Papadopoulos, A., 2012. Improving the representation of river–groundwater interactions in land surface modeling at the regional scale: observational evidence and parameterization applied in the Community Land Model. J. Hydrol. 420, 72–86.
Zeng, J., Li, J., Lu, X., Wei, Z., Shangguan, W., Zhang, S., et al., 2022. Assessment of global meteorological, hydrological and agricultural drought under future warming based on CMIP6. Atmospheric and Oceanic Science Letters 15 (1), 100143.
Zhang, S., Chen, J., 2021. Uncertainty in projection of climate extremes: a comparison of CMIP5 and CMIP6. Journal of Meteorological Research 35 (4), 646–662.
Zhao, T., Dai, A., 2015. The magnitude and causes of global drought changes in the twenty-first century under a low–moderate emissions scenario. J. Clim. 28 (11), 4490–4512.
Zhao, T., Dai, A., 2022. CMIP6 model-projected hydroclimatic and drought changes and their causes in the twenty-first century. J. Clim. 35 (3), 897–921.